arXiv:1301.6501v1 [cond-mat.str-el] 28 Jan 2013

Magnetic Impurity Affected by Spin-Orbit Coupling: Behavior near a Topological Phase Transition

F. M. Hu,[1] T. O. Wehling,[2,3] J. E. Gubernatis,[4] Thomas Frauenheim,[3] R. M. Nieminen[1]
[1] *COMP/Department of Applied Physics, Aalto University School of Science,*
P.O. Box 11100, FI-00076 Aalto, Espoo, Finland
[2] *Institute of Theoretical Physics, University of Bremen, Otto-Hahn-Allee 1, D-28359 Bremen, Germany*
[3] *Bremen Center for Computational Materials Science,*
University of Bremen, Am Fallturm 1a, D-28359 Bremen, Germany
[4] *Theoretical Division, Los Alamos National Laboratory, Los Alamos, New Mexico 87545, USA*

(Dated: January 29, 2013)

We investigate the effect of spin-orbit coupling on the behavior of magnetic impurity at the edge of a zigzag graphene ribbon by means of quantum Monte Carlo simulations. A peculiar interplay of Kane-Mele type spin-orbit and impurity-host coupling is found to affect local properties such as the impurity magnetic moment and spectral densities. The special helical nature of the topological insulator on the edge is found to affect nonlocal quantities, such as the two-particle and spin-spin correlation functions linking electrons on the impurity with those in the conduction band.

Introduction. Spin-orbit coupling (SOC) plays a central role in topological insulator (TI) materials [1], it opens a gap inside the bulk but supports the gapless electron states on the boundary. On the boundary of TI, impurity potential scattering is restricted by time-reversal symmetry [2, 3]: the backscattering among the electrons is allowed only if it is accompanied by a spin flip. This restriction gives rise to novel Kondo physics of magnetic impurities in TI [4, 5]. Accordingly, the behavior of magnetic impurities in host materials with SOC has recently attracted interest. In two-dimensional (2D) systems, several theoretical papers [6, 7] report that the presence of the SOC can in general protect impurity's magnetic moment from being totally screened. However, for the specific case of the Rashba coupling [8, 9] it has been reported that the SOC only makes a small or a high-order contribution to Kondo scaling.

In general, SOC and energies associated with the Kondo screening of magnetic impurities can be of the same order of magnitude. It remains to be explored what effects arise when crossing over from weak to strong SOC. In particular, the question of how the impurity behaves when the host undergoes a topological phase transition from a normal state to TI is an open.

In this paper, we consider an Anderson impurity on the edge of a zigzag graphene ribbon with a Kane-Mele type SOC gradually strengthened, so a topological phase transition occurs in the system. Using quantum Monte Carlo (QMC) simulations at finite temperature, we preform a comprehensive study on the properties of impurity. Calculating local physical quantities on the impurity site, such as the average double occupancy, magnetic moment, spin susceptibility and spectral densities, we find that in general the SOC can support the local moment formation. We see that in the case of zero or weak SOC, impurity is mainly dominated by its coupling with localized edge states, realizing a situation similar to the zero band width Anderson (ZBWA) model. In the case of strong SOC, the edge states are delocalized and the impurity behaves as a spin in a normal metal. This difference between strong and weak coupling also manifests itself in the dependence of the local moment on chemical potential, which in graphene can be tuned by a gate voltage. We also study nonlocal linking of the electrons on impurity with those in the conduction band. In nonlocal two-particle correlations, we observe a set of distinct spin-momentum relations which show the helical locking and interplay between backscattering and spin flip. This interplay signals the appearance of a topological phase in the host. Additionally, we find the spin rotation symmetry in spin-spin correlation functions to be partially broken by the SOC. This finding agrees with a previous study of an Anderson impurity in 2D helical metal with variational method that is valid for large Coulomb interaction [6]. In this work, we study the effect of electron-electron interaction over a wide region and document that the Coulomb interaction enhances the anisotropy in spin-spin correlation function and plays a complicated role in spin and momenta scattering.

Model and methods. Our starting point is the Hamiltonian $H = H_{\text{K-M}} + H_1 + H_2$ where $H_{\text{K-M}}$ is the Kane-Mele model for a zigzag edge graphene ribbon [11]. It has two pieces: $H_{\text{K-M}} = H_t + H_{\text{so}}$, with H_t being the usual nearest-neighbor hopping of tight-binding model in graphene

$$H_t = -t \sum_{<ij>,\sigma} (c^\dagger_{i,\sigma} c_{j,\sigma} + \text{H.c.}) - \mu \sum_{i,\sigma} c^\dagger_{i,\sigma} c_{i,\sigma},$$

and

$$H_{\text{so}} = \lambda \sum_{<<ij>>} (i\nu_{ij} c^\dagger_i s^z c_j + \text{H.c.})$$

H_{so} is the SOC term and s^z is the z Pauli matrix. H_{so} thus has opposite signs for opposite electron spins. The parameters $\nu_{ij} = -\nu_{ji} = \pm 1$ depend on the orientation of the two nearest neighbor bonds as the electron hops from site i to j: $\nu_{ij} = +1$ if the electron makes a left turn to the second bond. It is negative if it makes a right turn. H_1 is the impurity Hamiltonian

$$H_1 = \sum_\sigma (\varepsilon_d - \mu) d^\dagger_\sigma d_\sigma + U d^\dagger_\uparrow d_\uparrow d^\dagger_\downarrow d_\downarrow .$$

Here ε_d is the energy of the impurity orbital and U is Coulomb repulsion inhibiting the simultaneous occupancy of the orbital by two electrons. Finally H_2 describes the hybridization between impurity and one of atoms on the edge (located at A-sublattice site R_{a0}),

$$H_2 = V \sum_\sigma [c^\dagger_{a0,\sigma} d_\sigma + d^\dagger_\sigma c_{a0,\sigma}] .$$

Our principal computational tools are the single-impurity QMC algorithm [12] for computing the local thermodynamic properties of the impurity and the method of Bayesian statistical inference for computing spectral densities. The QMC naturally returns the imaginary-time Green's function $G_{d\sigma}(\tau > 0) = \langle d_\sigma(\tau) d^\dagger_\sigma \rangle$ of the impurity. With this Green's function, we can easily compute the magnetic quantities on the impurity site such as the expected values of magnet moment square $m_d^2 = \langle (d^\dagger_\uparrow d_\uparrow - d^\dagger_\downarrow d_\downarrow)^2 \rangle$, the doubly occupancy $n_{d\uparrow} n_{d\downarrow} = \langle d^\dagger_\uparrow d_\uparrow d^\dagger_\downarrow d_\downarrow \rangle$ and the static impurity spin susceptibility

$$\chi = \int_0^\beta d\tau \langle m_d(\tau) m_d(0) \rangle, \tag{1}$$

where $\beta = T^{-1}$, $m_d(\tau) = e^{\tau H} m_d(0) e^{-\tau H}$. Computing the imaginary-time Green's function also enables us to compute the spectral density $A(\omega) = \sum_\sigma A_\sigma(\omega)$ by numerically solving [16]

$$G_d(\tau) = \int_{-\infty}^{\infty} d\omega \frac{e^{-\tau\omega} A(\omega)}{e^{-\beta\omega} + 1} .$$

Local properties. To gain insight about the consequences of the SOC, we solved the Kane-Mele model on zigzag graphene ribbon numerically and obtained the localized density of states (LDOS). For the LDOS in Fig. 1(a), we see that when $\lambda = 0$, a sharp peak exists at the Dirac point ($E/t = 0$) suggesting the existence of a strongly localized state on the zigzag edge. When $\lambda \neq 0$, the central peaks becomes smooth, and at $\lambda = 0.2t$, their values near $E/t = 0$ approach a constant and thus near the Dirac point become similar to the LDOS in a normal metal. The SOC suppresses the LDOS and therefore weakens the localized states on the edge.

In Fig. 1, we show the QMC results of $n_{d\uparrow} n_{d\downarrow}$, m_d^2 and χ versus the chemical potential μ which can be tuned by an electric field. With $\varepsilon_d = -U/2$ fixed and $\mu = 0$ the impurity site is half filled, and thus the magnetic moment is driven by avoiding the possibility of double occupancy. We see that increasing the SOC results in the average double occupancy $n_{d\uparrow} n_{d\downarrow}$ decreasing because the SOC suppresses the effective hybridization between impurity and edge states. Near the Dirac point, the average local magnetic moments (both m_d^2 and χ) are enhanced by the SOC. We also note that with weak SOC, i.e., $0.0 < \lambda < 0.05t$, the maxima of m_d^2 and χ are not at $\mu = 0$ while for the large λ, they are at $\mu = 0$. We comment that with small SOC the localized states on the edge are antiferromagnetically coupled to impurity states below the Fermi energy, so shifting μ from zero can decouple these oppositely-aligned spin states and lead to the development of a magnet moment [13]. Contrary to the weak SOC case, strong SOC delocalizes the states and induces a flat LDOS on the edge, making the LDOS

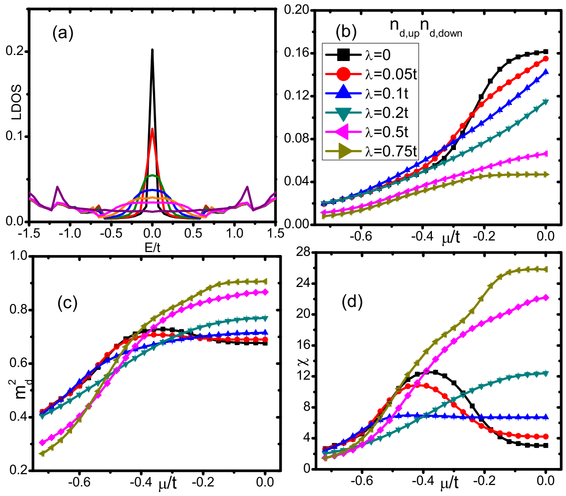

FIG. 1: (color online). (a) The LDOS as a function of energy E/t with different values for λ. From top to bottom $\lambda = 0$, $0.02t$, $0.04t$, $0.06t$, $0.08t$, $0.1t$ and $0.2t$. (b)-(c): $n_{d\mathrm{up}} n_{d\mathrm{down}}$, m_d^2, and χ versus μ/t. Here, $U = 1.2t$, $V = 0.65t$, $\varepsilon_d = -U/2$, and $T^{-1} = 32t^{-1}$.

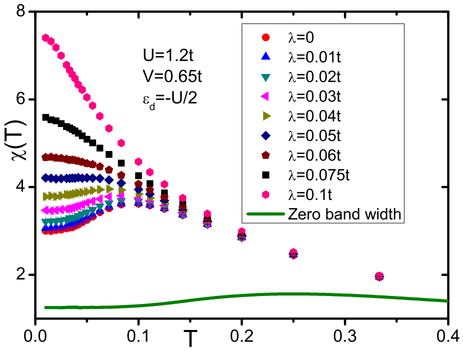

FIG. 2: (color online). The spin susceptibility χ as a function of T for different values of SOC. $U = 1.2t$, $V = 0.65t$ $\varepsilon_d = -U/2$ and $\mu = 0$. The solid line presents the results for ZBWA model.

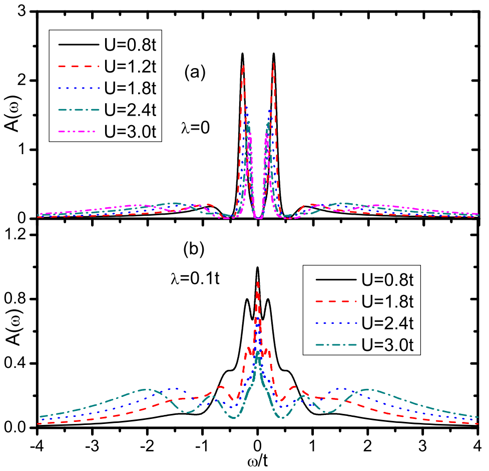

FIG. 3: (color online). The spectral density $A(\omega)$ versus ω/t. (a) The SOC $\lambda = 0$. The inset (a1) shows the position (absolute value) of two inner peaks versus $1/U$, and the inset (a2) shows the height of these two peaks versus $1/U^2$. (b) The SOC $\lambda = 0.1t$. In both figures, $V = 0.65t$, $\mu = 0$, $\varepsilon_d = -U/2$ and $T^{-1} = 32t^{-1}$.

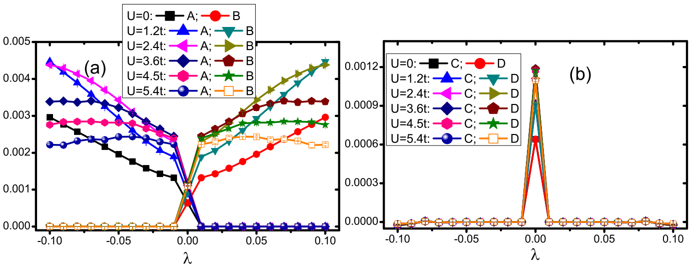

FIG. 4: (color online). In (a) correlation function A is $\langle c_{k,\uparrow} d^{\dagger}_{\uparrow} d_{\downarrow} c^{\dagger}_{-k,\downarrow}\rangle$ and B is $\langle c_{-k,\uparrow} d^{\dagger}_{\uparrow} d_{\downarrow} c^{\dagger}_{k,\downarrow}\rangle$. In (b) C is $\langle c_{k,\uparrow} d^{\dagger}_{\uparrow} d_{\downarrow} c^{\dagger}_{k,\downarrow}\rangle$ and D is $\langle c_{-k,\uparrow} d^{\dagger}_{\uparrow} d_{\downarrow} c^{\dagger}_{-k,\downarrow}\rangle$. In both figures, $V = 0.65t$, $\varepsilon_d = -U/2$, $\mu = 0$, $\beta = 32t^{-1}$ and momentum $k = 0.00125\pi$.

near the Fermi energy similar to that of a normal metal. Thus we see that half filling (hole-particle symmetry) optimizes the magnetic moment at $\mu = 0$.

Figure 2 shows the impurity spin susceptibility χ as a function of temperature for different values of λ. We fix hole-particle symmetry by setting $\mu = 0$ and $\varepsilon_d = -U/2$. Doing so means the average electron occupancy of the impurity site is one; i.e., it is half filled. From the figure, we also see that with small $0 < \lambda < 0.05t$ and the lowing of temperature, the spin susceptibility first increases, then decreases and finally saturates (totally screened). But when $0.05t < \lambda < 0.1t$, χ first increases and then directly becomes saturated. We note that when the SOC is gradually opened, χ goes cross over form the behavior in ZBWA model (solid line in Figure 2) to that in a normal metal [14]. We propose this transition occurs because of the edge states delocalized by the SOC.

In Fig. 3, we show additional spectral densities $A(\omega)$ for the impurity site. Here we have $A(\omega) = A(-\omega)$ due to hole-particle symmetry. In Fig. 3a are results for $\lambda = 0$. In this case the impurity states are strongly correlated with the edge states. There are four peaks. The inner two are from the localized edge state which is split by the impurity state. The outer two peaks are from the impurity level which is split by the Coulomb interaction into ε_d and $\varepsilon_d + U$. This four-peak structure is similar to that in ZBWA model. It is known that in ZBWA model the separations and weights of two inner peaks are proportional to U^{-1} and U^{-2}, respectively [14], but here we cannot see this dependence on U.

In Fig. 3b, we show $A(\omega)$ for $\lambda = 0.1t$. Clearly visible is the central Kondo resonance and the heights of two inner peaks decreasing with increasing λ. This behavior is consistent with the expectation that increasing λ weakens the localized states. We also see that when we increase U, the height of the central Kondo peak, as well as that of the two inner peaks, decrease, but the heights of the outer two peaks from impurity levels increase. These behaviors are similar to those of an impurity in normal metal. Additionally, the two smooth peaks around $\omega = \pm t$ are remnants of van Hove singularities.

Nonlocal properties. The most interesting property of a TI boundary is time-reversal invariance causing backscattering always being accompanied by spin-flip scattering. In order to directly see signatures of this phenomenon, we computed a set P_k of two-particle correlation functions between the impurity site and the conduction electron[15] with momentum k: $P_k = \{\langle c_{k,\uparrow} d^{\dagger}_{\uparrow} d_{\downarrow} c^{\dagger}_{-k,\downarrow}\rangle, \langle c_{-k,\uparrow} d^{\dagger}_{\uparrow} d_{\downarrow} c^{\dagger}_{k,\downarrow}\rangle, \langle c_{k,\uparrow} d^{\dagger}_{\uparrow} d_{\downarrow} c^{\dagger}_{k,\downarrow}\rangle, \langle c_{-k,\uparrow} d^{\dagger}_{\uparrow} d_{\downarrow} c^{\dagger}_{-k,\downarrow}\rangle\}$. In Fig. 4, we focus on the states with $k = \pm 0.00125\pi$ that are below Fermi energy. In Fig. 4a, we see that for positive λ, the correlation function $\langle c_{k,\uparrow} d^{\dagger}_{\uparrow} d_{\downarrow} c^{\dagger}_{-k,\downarrow}\rangle = 0$ while $\langle c_{-k,\uparrow} d^{\dagger}_{\uparrow} d_{\downarrow} c^{\dagger}_{k,\downarrow}\rangle \neq 0$, and with negative λ, the situation is opposite. This means that the conduction electrons with a fixed spin orientation can only move in one direction. When the sign of SOC changes, they then move in the opposite direction. Backscattering occurs if accompanied by a spin flip. In

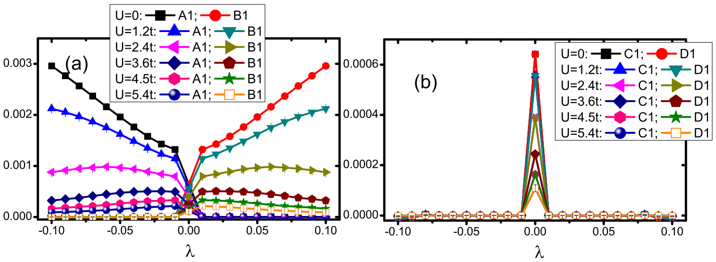

FIG. 5: (color online). In (a) correlation function A1 is $\langle c_{k,\uparrow} d^{\dagger}_{\uparrow}\rangle\langle d_{\downarrow} c^{\dagger}_{-k,\downarrow}\rangle$ and B1 is $\langle c_{-k,\uparrow} d^{\dagger}_{\uparrow}\rangle\langle d_{\downarrow} c^{\dagger}_{k,\downarrow}\rangle$. In (b) C1 is $\langle c_{k,\uparrow} d^{\dagger}_{\uparrow}\rangle\langle d_{\downarrow} c^{\dagger}_{k,\downarrow}\rangle$ and D1 is $\langle c_{-k,\uparrow} d^{\dagger}_{\uparrow}\rangle\langle d_{\downarrow} c^{\dagger}_{-k,\downarrow}\rangle$. The parameters are the same to those in Fig. 4.

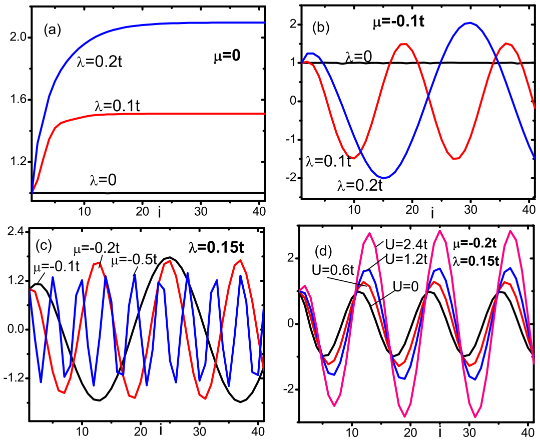

FIG. 6: (color online). The ratio S_i^x/S_i^z as a function of the position i on A-sublattice edge. (a) The non-doping case $\mu = 0$, (b) the doping case $\mu = -0.1t$, and (c) spin-orbit coupling $\lambda = 0.15t$ and the chemical potential is varied. In (a)-(c) $U = 1.2t$; in (d) $\mu = -0.2t$, $\lambda = 0.15t$ and U is varied. In all figures $V = 0.65t$, $\varepsilon_d = -U/2$ and $T^{-1} = 32t^{-1}$.

Fig. 4b, we observe that the two correlation functions $\langle c_{k,\uparrow} d_\uparrow^\dagger d_\downarrow c_{k,\downarrow}^\dagger \rangle$ and $\langle c_{-k,\uparrow} d_\uparrow^\dagger d_\downarrow c_{-k,\downarrow}^\dagger \rangle$ vanish, meaning that spin flip combined with forward scattering is forbidden in helical liquid phase.

To evaluate the effect of electron-electron correlation, we also computed the set $\bar{P}_k$ of products of two single-particle correlators, each corresponding a two-particle correlator P_k; for example, we computed the product $\langle c_{k,\uparrow} d_\uparrow^\dagger \rangle \langle d_\downarrow c_{-k,\downarrow}^\dagger \rangle$ that is part of $\langle c_{k,\uparrow} d_\uparrow^\dagger d_\downarrow c_{-k,\downarrow}^\dagger \rangle$. The difference between the two corresponding functions is just the vertex contributions of interaction [17]. We show the products of the two single-particle correlation functions in Fig. 5, and comparing Figs. 4 and 5, we can see the helical contributions to the two-particle correlations.

If we study the effect of the Coulomb interaction by varying U over a wide range and fixing $\varepsilon_d = -U/2$, the difference between a member of P_k and the corresponding member of $\bar{P}_k$ becomes more obvious. Figure 5 shows that the product of the two single-particle correlators monotonically decreases as U increases, while the two-particle correlators at first increase ($0 < U < 1.2t$) and then decrease ($U > 1.2t$). In fact we can enhance $\bar{P}_k$ by increasing $|\varepsilon_d - E_k|^{-1}$ (E_k is the energy of $\pm k$ states) and the impurity's double occupancy. U decreases these factors. While a member of P_k not only depends on coupling between the impurity level ε_d and $\pm k$ states but also depends on the impurity's moment. U at first develops the magnetic moment and then suppresses the SOC.

Using the same algorithm as those used for computing P_k and $\bar{P}_k$, we computed the spatial spin-spin correlation functions, $S_{\mathbf{i}}^z$, $S_{\mathbf{i}}^x$ and $S_{\mathbf{i}}^y$ defined as $S_{\mathbf{i}}^z = \langle (d_\uparrow^\dagger d_\uparrow - d_\downarrow^\dagger d_\downarrow)(c_{\mathbf{i}\uparrow}^\dagger c_{\mathbf{i}\uparrow} - c_{\mathbf{i}\downarrow}^\dagger c_{\mathbf{i}\downarrow}) \rangle$, $S_{\mathbf{i}}^x = \langle (d_\uparrow^\dagger d_\downarrow + d_\downarrow^\dagger d_\uparrow)(c_{\mathbf{i}\uparrow}^\dagger c_{\mathbf{i}\downarrow} + c_{\mathbf{i}\downarrow}^\dagger c_{\mathbf{i}\uparrow}) \rangle$,

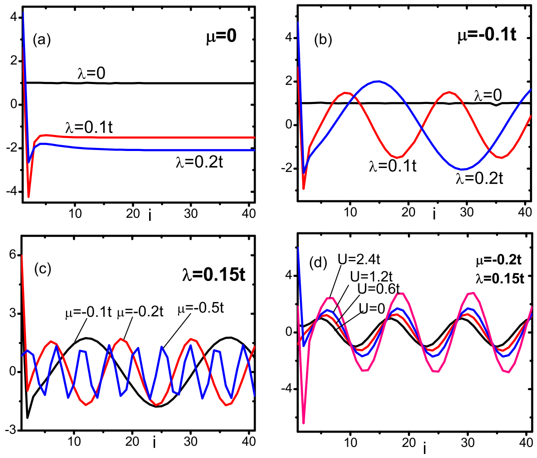

FIG. 7: (color online). The ratio S_i^x/S_i^z. Here i is a B-sublattice position on the edge. All the parameters are the same as those in Fig. 6.

and $S_{\mathbf{i}}^y = (-i)^2 \langle (d_\uparrow^\dagger d_\downarrow - d_\downarrow^\dagger d_\uparrow)(c_{\mathbf{i}\uparrow}^\dagger c_{\mathbf{i}\downarrow} - c_{\mathbf{i}\downarrow}^\dagger c_{\mathbf{i}\uparrow}) \rangle$. We find that the spin rotational symmetry in these correlations is partly broken by the SOC, i.e., $S_{\mathbf{i}}^z \neq S_{\mathbf{i}}^x$ but $S_{\mathbf{i}}^y = S_{\mathbf{i}}^x$, and that this asymmetry agrees with what was found for an impurity in the two-dimensional helical metal [6].

In Figs. 6 and 7, we display this anisotropy by plotting the ratio $S_{\mathbf{i}}^x/S_{\mathbf{i}}^z$ on the two sublattices. It is clear that the behaviors on two sub-lattices are similar but independent: the ratio equals one when $\lambda = 0$, but when $\lambda \neq 0$, the ratio S_i^x/S_i^z has a large distance asymptotic behavior $\sim \alpha \sin(2\beta R_i)$. Here R_i denotes a site on the zigzag edge. The two parameters α and β depend on the SOC, Coulomb interaction and chemical potential. The magnitude of α increases as λ and U increase, meaning that SOC and electron-electron interaction enhances the anisotropy in spatial correlation functions. Further, β equals π when $\mu = 0$ or $\lambda = 0$, and it decreases as λ increases but increases as μ moves below zero.

Discussion and conclusion. In this paper, we study an Anderson impurity on a zigzag graphene ribbon undergoing a topological phase transition driven by a Kane-Mele type SOC. Using QMC simulations, we investigate both the local and non-local properties of the impurity. We find that with the SOC increasing from zero, the formation of local moment is supported and the impurity behavior crosses over from a spin in a band with zero width to one in a normal metal. This is because SOC delocalizes states on the edge. As for non-local properties, we clearly see the helical locking and the collaboration of backscattering and spin flip in the two-particle correlators and find a broken spin rotation symmetry in spin-spin correlation functions.

Although the intrinsic SOC of carbon atoms is weak [18], a strong SOC can be achieved by heavy-atom doping[19–23] and tuned by a gate bias [24]. The magnetic impurity could be realized by dangling σ bonds in graphene [25]. Several physical quantities discussed can be experimentally measured: scanning tunneling microscope (STM) can measure $A(\omega)$, and recent developments in the field of spin-polarized STM [26] open the possibility to detect the spin-spin correlations.

Acknowledgement. This work was supported by Academy of Finland through its Center of Excellence (2012-2017) program. The work of JEG was supported by the US Department of Energy. We acknowledge computational resources from CSC-IT Center for Science Ltd and Aalto local cluster Triton. FMH is grateful to BC-CMS for hospitality during the visit.

[1] Xiao-Liang Qi and Shou-Cheng Zhang, Rev. Mod. Phys. **83**, 1057 (2011).
[2] C. Wu, B. A. Bernevig, and S. C. Zhang, Phys. Rev. Lett. **96**, 106401 (2006).
[3] C. Xu and J. E. Moore, Phys. Rev. B **73**, 045322 (2006).
[4] Joseph Maciejko, Chaoxing Liu, Yuval Oreg, Xiao-Liang Qi, Congjun Wu, and Shou-Cheng Zhang, Phys. Rev. Lett. **102**, 256803 (2009).
[5] Yoichi Tanaka, A. Furusaki, and K. A. Matveev, Phys. Rev. Lett. **106**, 236402 (2011).
[6] Xiao-Yong Feng, Wei-Qiang Chen, Jin-Hua Gao, Qiang-Hua Wang, and Fu-Chun Zhang, Phys. Rev. B **81**, 235411 (2010).
[7] L. Isaev, D. F. Agterberg, and I. Vekhter, Phys. Rev. B **85**, 081107 (2012).
[8] Rok Žitko and Janez Bonča, Phys. Rev. B **84**, 193411 (2011).
[9] Mahdi Zarea, Sergio E. Ulloa, and Nancy Sandler, Phys. Rev. Lett. **108**, 046601 (2012).
[10] Katsunori Wakabayashi, Mitsutaka Fujita, Hiroshi Ajiki, and Manfred Sigrist, Phys. Rev. B **59**, 8271 (1999).
[11] C. L. Kane and E. J. Mele, Phys. Rev. Lett. **95**, 226801 (2005).
[12] J. E. Hirsch and R. M. Fye, Rev. Phys. Rev. Lett. **56**, 2521 (1986).
[13] F. M. Hu, J. E. Gubernatis, Hai-Qing Lin, Yan-Chao Li, and R. M. Nieminen, Phys. Rev. B **85**, 115442 (2012).
[14] A. C. Hewson, *The Kondo Problem to Heavy Fermions* (Cambridge University Press, Cambridge, 1993).
[15] J. E. Gubernatis, J. E. Hirsch, and D. J. Scalapino, Phys. Rev. B **35**, 8478 (1987).
[16] M. Jarrell and J. E. Gubernatis, Phys. Rept. **269**, 133 (1996).
[17] S. R. White, D. J. Scalapino, R. L. Sugar, N. E. Bickers, and R. T. Scalettar, Phys. Rev. B **39**, 839 (1989).
[18] Daniel Huertas-Hernando, F. Guinea, and Arne Brataas, Phys. Rev. B **74**, 155426 (2006).
[19] A. H. Castro Neto and F. Guinea, Phys. Rev. Lett. **103**, 026804 (2009).
[20] Samir Abdelouahed, A. Ernst, J. Henk, I. V. Maznichenko, and I. Mertig, Phys. Rev. B **82**, 125424 (2010).
[21] Zhenhua Qiao, Shengyuan A. Yang, Wanxiang Feng, Wang-Kong Tse, Jun Ding, Yugui Yao, Jian Wang, and Qian Niu, Phys. Rev. B **82**, 161414(R) (2010).
[22] Conan Weeks, Jun Hu, Jason Alicea, Marcel Franz, and Ruqian Wu , Phys. Rev. X **1**, 021001 (2011).
[23] Jun Ding, Zhenhua Qiao, Wanxiang Feng, Yugui Yao, and Qian Niu, Phys. Rev. B **84**, 195444 (2011).
[24] Zhuoyu Chen, Hongtao Yuan, Yanfeng Zhang, Kentaro Nomura, Teng Gao, Yabo Gao, Hidekazu Shimotani, Zhongfan Liu , and Yoshihiro Iwasa, Nano Lett., **12**, 2212 (2012).
[25] M. A. Cazalilla, A. Iucci, F. Guinea, and A. H. Castro Neto, arXiv:1207.3135 (2012).
[26] Lihui Zhou, Jens Wiebe, Samir Lounis, Elena Vedmedenko, Focko Meier, Stefan Blügel, Peter H. Dederichs and Roland Wiesendanger, Nature Physics, **6**, 187 (2010).